THE UNIVERSITY OF
WARWICK

Original citation:
Tian, Y. and Zhao, C.Y. (2011). A numerical investigation of heat transfer in phase change materials (PCMs) embedded in porous metals. Energy, 36(9), pp. 5539-5546.
Permanent WRAP url:
http://wrap.warwick.ac.uk/39277

warwickpublicationswrap

highlight your research

http://go.warwick.ac.uk/lib-publications

A Numerical Investigation of Heat Transfer in Phase Change Materials (PCMs) Embedded in Porous Metals

Y. Tian, C.Y. Zhao[*]

School of Engineering, University of Warwick, CV4 7AL, United Kingdom
*Corresponding author, Email: C.Y.Zhao@warwick.ac.uk
Tel: +44 (0)2476522339, Fax: +44 (0)24 7641 8922

ABSTRACT

The effects of metal foams on heat transfer enhancement in Phase Change Materials (PCMs) are investigated. The numerical investigation is based on the two-equation non-equilibrium heat transfer model, in which the coupled heat conduction and natural convection are considered at phase transition and liquid zones. The numerical results are validated by experimental data. The main findings of the investigation are that heat conduction rate is increased significantly by using metal foams, due to their high thermal conductivities, and that natural convection is suppressed owing to the large flow resistance in metal foams. In spite of this suppression caused by metal foams, the overall heat transfer performance is improved when metal foams are embedded into PCM; this implies that the enhancement of heat conduction offsets or exceeds the natural convection loss. The results indicate that for different metal foam samples, heat transfer rate can be further increased by using metal foams with smaller porosities and bigger pore densities.

NOMENCLATURE

a_{sf} = specific surface area — m^{-1}

C_f = inertia coefficient of fluid flow in metal foams — (dimensionless)

C_p = specific heat at constant pressure — $\text{KJ/(Kg}\,^{\circ}\text{C)}$

C_{ps} = specific heat of metal at constant pressure — $\text{KJ/(Kg}\,^{\circ}\text{C)}$

C_{pf} = specific heat of PCM at constant pressure — $\text{KJ/(Kg}\,^{\circ}\text{C)}$

d_f = equivalent diameter of metal fibre — m

d_p = equivalent pore size — m

e = length ratio of cubic juncture node to ligament — (dimensionless)

$\mathbf{g}$ = gravity vector — m/s^2

H_L = latent heat of fusion — KJ/Kg

h_1 = heat transfer coefficients at the left boundary — $\text{W/(m}^2\text{K)}$

h_2 = heat transfer coefficients at the right boundary — $\text{W/(m}^2\text{K)}$

h_3 = heat transfer coefficients at the top boundary — $\text{W/(m}^2\text{K)}$

h_{sf} = interstitial heat transfer coefficient — $\text{W/(m}^2\text{K)}$

K = permeability — m^2

k_{fe} = effective thermal conductivity without metal — W/(mK)

k_{se} = effective thermal conductivity without fluid — W/(mK)

L_1 = length of the PCM sample in x-axis — m

L_2 = length of the PCM sample in y-axis — m

P = pressure — Pa

q_w = heat flux — W/m^2

t = time — s

$T(x,y,t)$ = temperature function — $^{\circ}\text{C}$

T_0 = initial temperature — $^{\circ}\text{C}$

T_f = temperature of surrounding fluids °C

T_m = fusion temperature °C

U = equivalent thermal conductivity W/(mK)

u = the component of the velocity **V** in x-direction m/s

v = the component of the velocity **V** in y-direction m/s

V = velocity vector m/s

SUBSCRIPTS

e = effective value

f = fluid (PCM)

fe = effective value for PCM

ref = reference value

s = metal foam

se = effective value for metal foam

GREEK

β = thermal expansion coefficient K^{-1}

ε = porosity (percentage)

λ = ratio of ligament radius to ligament length (dimensionless)

ρ = density Kg/m^3

μ_f = dynamic viscosity Pa s

∇ = Laplace operator

1. Introduction

Most renewable energy sources are intermittent, so there inevitably exists a time discrepancy between energy demand and generation. Because of this, thermal energy storage (TES) [1] has become an indispensable technology, playing a pivotal role in those applications involving renewable energy. TES technologies rely on high-quality materials with desirable heat storage capacity and excellent heat transfer performance. Phase change materials (PCMs), which release or absorb thermal energy during melting and solidification processes, are believed to have outstanding capability to store a massive amount of heat efficiently during their phase change processes [1, 2]. PCMs have been investigated in building applications [3–6], industrial waste heat recovery [7], solar collectors [8], solar power plants [9], high-efficient compact heat sinks [10], solar cookers [11, 12] and solar stills [13]. Thermal stability investigations of PCMs have been conducted through implementing repeated thermal cycle tests [14, 15].

Thermal energy storage can be generally classified as either sensible heat storage or latent heat storage. Latent heat storage is particularly attractive, not only because is it able to provide higher energy storage density, but also it can store thermal energy as the latent heat of fusion at constant temperature (phase change temperature of the corresponding PCMs). This is of great importance in those applications requiring stable working temperatures, for example the high temperature and high pressure steam used in power plant to propel turbo-generators.

However, most PCMs suffer from the common problem of low thermal conductivities, being around 0.2 W/(mK) for most paraffin waxes [1, Table 4] and 0.5 W/(mK) for most inorganic salts [1, Table 1]. This prolongs the charging and discharging period of TES systems. Therefore, a heat transfer enhancement technology in PCMs is needed [16–19]. Metal foams [20, 21], which have high strength-to-density ratio, ultralight porous structure and relatively high thermal conductivity, are believed to be a promising material for enhancing heat transfer performance and reducing the charging and discharging periods of PCMs. Several investigations have been carried out for heat transfer in metal foams, but most have been restricted to single-phase heat transfer problems [20–24]. For solid/liquid phase change heat transfer in metal foams, there are only a few publications

4

giving experimental test data for the latent thermal energy storage [18, 25]. Although the Ref. [18] also presented a thermal analysis of solid/liquid phase change heat transfer in PCMs embedded with metal foams, but it was based on heat conduction only without natural convection being taken into account.

The present paper provides a two-dimensional thermal analysis of coupled heat conduction and natural convection for PCMs embedded inside copper foams with different microstructures. The traditional one-equation thermal equilibrium model [20] treats metal ligaments and PCMs with the same temperature, and is only applicable to those porous media in which the two different phases do not have large differences in thermal conductivity. However, the thermal conductivity of metal ligaments is generally several thousand times higher than that of PCMs inside metal foams (with pure copper being round 350 W/m/K and paraffin wax being around 0.2 W/m/K). The traditional one-equation model based on the assumption of local thermal equilibrium cannot therefore be transplanted mechanically to metal foams [26, 27].

The two-equation non-thermal equilibrium model developed in this paper takes into account the temperature differences between metal ligaments and PCMs. The model also includes porosity of the materials as a factor. It is important to note that metal foams have much higher porosity (usually at least 90%) than packed beds (usually in the range of 40%–60%) [22].

2. Problem description

The physical problem to be tackled in this study is depicted schematically in Fig. 1. The PCM is impregnated in a piece of rectangular copper foam. The PCM and the foam are heated from the bottom side through a constant heat flux q_w provided by an electric heater. Because perfect insulation is hard to achieve in real applications, they lose heat to the atmosphere through the left, right and top boundaries, with heat loss coefficients h_1, h_2 and h_3 respectively. The curve in Fig. 1 represents the melting front of the PCM during phase change, so within the area below this curve, the PCM has been fully melted into liquid state, whilst within the area above this curve, the PCM is solid.

3 Mathematical model

3.1 Equations of fluid dynamics

In the model developed in this paper, a volume-averaging technique is employed, for which the classical Continuity Equation is:

$$\nabla \bullet \langle \mathbf{V} \rangle = \mathbf{0} \tag{1}$$

Here, $\langle \ \rangle$ denotes the volume-averaged value of a certain function over an REV (Representative Elementary Volume inside metal foams) [20]. The Continuity Equation takes on different forms under different coordinate systems, and its form under the Cartesian coordinate system can be written by:

$$\frac{\partial u}{\partial x} + \frac{\partial v}{\partial y} = 0 \tag{2}$$

Here, u and v denote the components of the velocity $\mathbf{V}$ in x-direction and in y-direction respectively.

Based on the Brinkman-Forchheimer extended Darcy model, the Momentum Equation is given by:

$$\frac{1}{\varepsilon} \langle \rho_f \rangle \frac{\partial \mathbf{V}}{\partial t} + \frac{\langle \rho_f \rangle}{\varepsilon^2} \langle (\mathbf{V} \bullet \nabla) \mathbf{V} \rangle =$$
$$-\nabla \langle P \rangle + \frac{\mu_f}{\varepsilon} \nabla^2 \langle \mathbf{V} \rangle - \frac{\mu_f}{K} \langle \mathbf{V} \rangle - \frac{\rho_f C_f}{\sqrt{K}} \| \langle \mathbf{V} \rangle \| \langle \mathbf{V} \rangle + \langle \rho_f \rangle \mathbf{g} \tag{3}$$

Here, $\| \ \|$ denotes the norm of a vector, $\mathbf{g}$ denotes the gravity vector, ε denotes the porosity of the metal foam, μ_f denotes the dynamic viscosity of the PCM, ρ_f denotes the density of the PCM, K is the permeability coefficient for homogeneous metal foams, which can be a vector/tensor for anisotropic materials, and C_f denotes the inertial factor for fluid flow in metal foams.

The Momentum Equations for u and v are given by:

$$\rho_f \frac{\partial u}{\partial t} + \frac{\rho_f}{\varepsilon}\left(u\frac{\partial u}{\partial x} + v\frac{\partial u}{\partial y}\right) =$$

$$-\frac{\partial p}{\partial x} + \frac{\mu_f}{\varepsilon}\left(\frac{\partial^2 u}{\partial x^2} + \frac{\partial^2 u}{\partial y^2}\right) - \frac{\mu_f}{K}u - \frac{\rho_f C_f}{\sqrt{K}}|u|u \tag{4}$$

$$\rho_f \frac{\partial v}{\partial t} + \frac{\rho_f}{\varepsilon}\left(u\frac{\partial v}{\partial x} + v\frac{\partial v}{\partial y}\right) =$$

$$-\frac{\partial p}{\partial y} + \frac{\mu_f}{\varepsilon}\left(\frac{\partial^2 v}{\partial x^2} + \frac{\partial^2 v}{\partial y^2}\right) - \frac{\mu_f}{K}v - \frac{\rho_f C_f}{\sqrt{K}}|v|v + \rho_f g\varepsilon\beta(T_f - T_{ref}) \tag{5}$$

Here, β denotes the thermal expansion coefficient of the PCM and T_f denotes the temperature of the PCM. The last term on the right hand side of Eq. (5) represents the buoyancy force [24] caused by temperature differences of the PCM, and it is the driving force of the natural convection. The intensity of the natural convection in the PCM mainly depends on two factors: its driving force and its resisting force. The driving force increases with increasing temperature differences, whilst the resisting force can be reduced by decreasing the viscosity μ_f of the PCM. With fixed temperature differences, the latter results in natural convection weakening when the viscosity of the PCM is increased. When the PCM is still in solid state, its viscosity is infinite, so that natural convection does not take place, but as the PCM becomes liquid after melting finishes, the viscosity falls rapidly, so that natural convection can take place.

3.2 Equations of phase change heat transfer

In order to cope with the phase change heat transfer problem, the enthalpy method has been employed in this study. The relationship between PCM enthalpy function $H_f(x,y,t)$ and temperature $T_f(x,y,t)$ is given by:

$$T_f = \begin{cases} \dfrac{H_f}{\rho_f C_{pf}}, & H_f \in (-\infty, \rho_f C_{pf}T_m) \\ T_m, & H_f \in [\rho_f C_{pf}T_m, \rho_f C_{pf}T_m + \rho_f H_L] \\ \dfrac{H_f - \rho_f H_L}{\rho_f C_{pf}}, & H_f \in (\rho_f C_{pf}T_m + \rho_f H_L, +\infty) \end{cases} \tag{6}$$

The Energy Equation for the metal foam [20] is given by:

$$\langle \rho_s \rangle C_{ps} \frac{\partial \langle T_s(x,y,t) \rangle}{\partial t} = \langle \nabla \bullet \left[k_{se} \nabla \langle T_s(x,y,t) \rangle \right] \rangle \\ - h_{sf} a_{sf} \left[\langle T_s(x,y,t) \rangle - \langle T_f(x,y,t) \rangle \right] \tag{7}$$

With the enthalpy method being used in the present paper, the Energy Equation for the PCM is given by:

$$\frac{\partial \langle H_f(x,y,t) \rangle}{\partial t} + \langle \rho_f \rangle C_{pf} \mathbf{V} \bullet \nabla \langle T_f(x,y,t) \rangle = \\ \langle \nabla \bullet \left[k_{fe} \nabla \langle T_f(x,y,t) \rangle \right] \rangle + h_{sf} a_{sf} \left[\langle T_s(x,y,t) \rangle - \langle T_f(x,y,t) \rangle \right] \tag{8}$$

Here, k_{se} denotes effective thermal conductivity of the metal foam, k_{fe} denotes effective thermal conductivity of the PCM, h_{sf} denotes inter-phase heat transfer coefficient between metal ligaments and PCM, and a_{sf} is specific surface area of the metal foam. The values of these parameters for metal foam microstructures are obtained by employing the model by Calmidi and Mahajan [20, 22].

Under the Cartesian coordinate system, the above Energy Equations for the metal foam and the PCM are given by Eqs. (9) and (10) respectively:

$$\rho_s C_{ps} (1-\varepsilon) \frac{\partial T_s}{\partial t} = k_{se} \left(\frac{\partial^2 T_s}{\partial x^2} + \frac{\partial^2 T_s}{\partial y^2} \right) - h_{sf} a_{sf} \left[T_s - T_f \right] \tag{9}$$

$$\varepsilon \frac{\partial H_f}{\partial t} + \rho_f C_{pf} \varepsilon \left(u \frac{\partial T_f}{\partial x} + v \frac{\partial T_f}{\partial y} \right) = k_{fe} \left(\frac{\partial^2 T_f}{\partial x^2} + \frac{\partial^2 T_f}{\partial y^2} \right) \\ + h_{sf} a_{sf} \left[T_s - T_f \right] \tag{10}$$

3.3 The initial and boundary conditions

The initial and boundary conditions for u, v, T_s, T_f are shown in the following equations. Eq. (11) is obtained from the velocity non-slip principle. Eq. (12) gives the initial conditions for PCM and metal foam. The boundary conditions for the system are given by Eqs. (13) and (14) (lower boundary, which is the heating surface), Eqs. (15) and (16) (left boundary), Eqs (17) and (18) (right boundary) and Eqs (19) and (20) (upper boundary).

$$u,v\big|_{x=0,L_1} = 0, \ u,v\big|_{y=0,L_2} = 0 \tag{11}$$

$$u,v\big|_{t=0} = 0, \ T_s\big|_{t=0} = T_f\big|_{t=0} = T_0 \tag{12}$$

$$k_{se}\frac{\partial T_s}{\partial y}\bigg|_{y=0} + k_{fe}\frac{\partial T_f}{\partial y}\bigg|_{y=0} = -q_w \tag{13}$$

$$T_f\big|_{y=0} = T_s\big|_{y=0} \tag{14}$$

$$k_{se}\frac{\partial T_s}{\partial x}\bigg|_{x=0} + h_1(1-\varepsilon)\Big[T_\infty - T_s\big|_{x=0}\Big] = 0 \tag{15}$$

$$k_{fe}\frac{\partial T_f}{\partial x}\bigg|_{x=0} + h_1\varepsilon\Big[T_\infty - T_f\big|_{x=0}\Big] = 0 \tag{16}$$

$$-k_{se}\frac{\partial T_s}{\partial x}\bigg|_{x=L_1} + h_2(1-\varepsilon)\Big[T_\infty - T_s\big|_{x=L_1}\Big] = 0 \tag{17}$$

$$-k_{fe}\frac{\partial T_f}{\partial x}\bigg|_{x=L_1} + h_2\varepsilon\Big[T_\infty - T_f\big|_{x=L_1}\Big] = 0 \tag{18}$$

$$-k_{se}\frac{\partial T_s}{\partial y}\bigg|_{y=L_2} + h_3(1-\varepsilon)\Big[T_\infty - T_s\big|_{y=L_2}\Big] = 0 \tag{19}$$

$$-k_{fe}\frac{\partial T_f}{\partial y}\bigg|_{y=L_2} + h_3\varepsilon\Big[T_\infty - T_f\big|_{y=L_2}\Big] = 0 \tag{20}$$

3.4 Modeling of metal foam microstructures

There are still several important parameters for metal foam microstructures that need to be determined for solving the equations of fluid dynamics and phase change heat transfer. They are permeability, inertial factor, pore size, metal fiber diameter, effective thermal conductivity, surface area density, and inter-phase heat transfer coefficient. The determination of these parameters is complicated and strongly depends on special microstructures inside metal foams. Several existing models presented by previous researchers are employed in this study to obtain these parameters. For simplicity, this subsection only gives the computational formula for effective thermal conductivity,

permeability, inertial factor and surface area density. The detailed derivation of all other parameters is given in [20, 22, 28].

Calmidi and Mahajan [20, 22] presented a 2D simplified model of effective thermal conductivity for metal foams, which gave good agreement with test data. However the real microstructures in metal foams are three-dimensional, and therefore a 3D model is preferred in order to get improved accuracy. In this paper, a 3D structured model (tetrakaidecahedron) presented by Boomsma and Poulikakos [23] has been used to deal with the effective thermal conductivity of metal foams (validated on metal foams with porosities from 88%-98%), which is shown in Eqs. (21) to (27):

$$k_e = \frac{\sqrt{2}}{2\left(R_A + R_B + R_C + R_D\right)} \tag{21}$$

$$R_A = \frac{4\lambda}{\left(2e^2 + \pi\lambda(1-e)\right)k_s + \left(4 - 2e^2 - \pi\lambda(1-e)\right)k_f} \tag{22}$$

$$R_B = \frac{\left(e - 2\lambda\right)^2}{(e - 2\lambda)e^2 k_s + \left(2e - 4\lambda - (e - 2\lambda)e^2\right)k_f} \tag{23}$$

$$R_C = \frac{\left(\sqrt{2} - 2e\right)^2}{2\pi\lambda^2\left(1 - 2e\sqrt{2}\right)k_s + 2\left(\sqrt{2} - 2e - \pi\lambda^2\left(1 - 2e\sqrt{2}\right)\right)k_f} \tag{24}$$

$$R_D = \frac{2e}{e^2 k_s + \left(4 - e^2\right)k_f} \tag{25}$$

$$\lambda = \sqrt{\frac{\sqrt{2}\left(2 - (5/8)e^3\sqrt{2} - 2\varepsilon\right)}{\pi\left(3 - 4e\sqrt{2} - e\right)}} \tag{26}$$

$$e = 0.339 \tag{27}$$

By employing data fitting technology, Calmidi and Mahajan [22] also obtained the empirical formula for permeability and inertial factor calculations of metal foams. Since their results showed good agreement with test data, so this present paper has employed their formula, with Eq. (28) showing permeability and Eq. (29) showing inertial factor respectively:

$$\frac{K}{d_p{}^2} = 0.00073(1-\varepsilon)^{-0.224}\left(\frac{d_f}{d_p}\right)^{-1.11} \tag{28}$$

$$C_f = 0.00212(1-\varepsilon)^{-0.132}\left(\frac{d_f}{d_p}\right)^{-1.63} \tag{29}$$

The surface area density of metal foams a_{sf} is defined as the total surface area (m^2) of metal fibres per unit volume (m^3), and it can be obtained by assuming that all metal fibres have an ideal cylindrical shape [22]. The formula presented by Calmidi and Mahajan [22] is given in Eq. (30):

$$a_{sf} = \frac{3\pi d_f\left(1-e^{-\left((1-\varepsilon)/0.04\right)}\right)}{\left(0.59 d_p\right)^2} \tag{30}$$

4. Numerical procedure

A FVM-based (Finite Volume Method) program has been developed for tackling with the aforementioned phase change heat transfer problem for PCMs embedded into metal foams. Coupled heat conduction and natural convection equations were solved simultaneously by employing the SIMPLE algorithm [29] in the uniform mesh grids. The independence of the accuracy of the numerical solution on the mesh size was also examined, and it was found that a uniform mesh grid of 50×200, in y-direction (0.025 m) and x-direction (0.2 m) respectively, can ensure that the numerical solution is mesh-independent, i.e., the calculation accuracy cannot be further improved by using a finer mesh grid.

The numerical programming needs to ensure that natural convection only takes place at the grids where the PCM is in its liquid state and does not take place at the grids where the PCM is still in its solid state. This is realised by only assigning the real viscosity value to the grids where the PCM is liquid whilst assigning a viscosity with the value of 10^{10} to the grids where the PCM is still solid.

5. Results and discussion

5.1 Experimental test rig and results

The experiment setup is shown schematically in Fig. 2. The test section comprises a piece of rectangular metal foam (copper foam with the dimension of 200×120×25 mm) with paraffin wax RT58 embedded in it. According to the PCM provider RUBITHERM®, the thermo-physical properties of RT58 are melting temperature: 48-62°C, latent heat of fusion: 181 kJ/kg, specific heat: 2.1 kJ/kg, dynamic viscosity: 0.0269 Pa·s, thermal conductivity: 0.2 W/m/K, thermal expansion coefficient: $1.1×10^{-4}$ K^{-1}. The metal foam was sintered onto a thin copper plate from the bottom side for better thermal contact. Attached to the copper plate is an electrical heater which is made of flexible silicon with adjustable heat flux, providing continuous and uniform heat flux for the PCM and metal foam. The heater input power can be precisely controlled and measured by a Variac and an electrical power meter (Hameg HM8115-2, accuracy ±0.5%). This allows the heat flux used in the test to be calculated through dividing the input power by the surface area of the copper plate.

In this test, nine thermocouples (accuracy ±0.1°C) were placed at different locations (y = 8 mm, 16 mm and 24 mm respectively, 3 thermocouples were used for each place to get more reliable readings) inside the PCM to monitor the transient temperature variation. Three thermocouples were placed on the copper plate to record the plate temperatures (y = 0 mm). Although perfect insulation cannot be guaranteed in the test, the underneath of the heating surface was insulated with Armflex insulation material and other surfaces were insulated by acrylic sheets which were transparent for observation during the tests. The temperatures and the input power were automatically recorded by a data acquisition system. From previous work by the authors [18], the overall uncertainty of the test was estimated at 6.67%.

The comparison between the pure RT58 sample and two metal-foam samples during melting process (charging) is shown in Fig. 3 ($\Delta T = T_{y=0\,mm} - T_{y=8\,mm}$), from which it can be seen that the heat transfer enhancement of metal foam on solid/liquid phase change heat transfer in PCM is very significant compared to the results of the pure PCM sample, especially at the solid zone. The heat transfer rate can be enhanced by 5-20 times. When

the PCM starts melting, natural convection takes place and it improves the heat transfer performance, thereby reducing the temperature difference between the wall and PCM. Even so, the addition of the metal foam can increase the overall heat transfer rate 3-10 times (depending on the metal foam structures) during the melting process (two-phase zone) and the liquid zone. It can also be concluded from Fig. 3 that the metal foam sample with larger relative density (namely smaller porosity) has better heat transfer performance than the one with smaller relative density. This is reasonable because larger relative density means larger percentage of metal skeleton, which is helpful for transferring heat from heating plate to the PCM more effectively.

5.2 Comparison between experimental data and numerical results

The numerical results and the corresponding experimental data are compared in Fig. 4 for $y = 0$ and 8 mm; y is the vertical coordinate in the computational domain, namely the distance between different locations and heating plate. Both numerical results and experimental data show that the PCM begins to melt around $t = 1200$s and finish phase change around $t = 4000$s. There is good agreement between numerical results and experimental data, and the most probable reason for the small discrepancies between them is that it has been assumed in the model that the PCM has a fixed melting point, similarly to crystal materials. In practice, is important to note that, RT58 melts in a temperature range of 48-62ºC (according to RUBITHERM[®]).

As shown in Fig. 4, the temperatures of RT58 increase more slowly after melting begins, because the heat provided is mainly used for phase change rather than increasing sensible heat. After the state of RT58 has become fully liquid (when temperatures are higher than 62ºC), its temperatures begin to increase more rapidly again, because the heat provided is now all used for increasing sensible heat of the PCM.

5.3 Flow field in natural convection

Figure 5 and Figure 6 present the velocity profiles at two different times ($t = 1108.3$s and 5859.0s, respectively), from which it can be clearly seen that two symmetrical eddies are formed when natural convection takes place. Both figures indicate that while the PCM near the symmetrical plane ($x = 0.1$) tends to move upward, the PCM on both the left and right sides has downward velocities. This is because the PCM can be regarded as

being insulated on the symmetrical plane (at $x = 0.1$), but that it is losing heat to atmosphere on both sides. In Fig. 5, only a small part of PCM has been melted and starts natural convection. As time goes on, more and more PCM is being melted. Fig. 6 shows the velocity profile when the PCM is fully melted.

From the numerical investigations, the velocities caused by buoyancy force are quite low, with an order of magnitude of 10^{-5} m/s. At first sight, this may seem rather surprising, but it is still believed to be reasonable, for the following reason. The buoyancy force term $\rho_f g \beta \Delta T$, which drives natural convection, has an order of magnitude of 10^1, but in the main drag force term $-\mu_f u / K$ (i.e. Darcy term), μ_f / K has an order of magnitude of 10^6. According to the equilibrium of forces, drag force should have a similar order of magnitude to buoyancy force, and therefore u should have an order of magnitude of 10^{-5}. The paraffin wax RT58 used in this study has high dynamic viscosity of 0.0269 Pa·s (1000 times higher than air) and low thermal expansion coefficient of $1.1*10^{-4}$ K^{-1} (30 times lower than air), so these special physical characteristics result in the velocity driven by buoyancy force being so small in this case. Since it is small, the natural convection fails to produce dominant influence on heat transfer. The similar suppression of natural convection was also found by Stritih [30], who added 32 metal fins into PCM to enhance heat transfer. However, he found that the addition of metal fins did not have the desired effects on heat transfer enhancement during melting, with the reason being that natural convection was significantly suppressed by the metal fins, so that the Rayleigh number in his study was not sufficiently high to overcome the large flow resistance.

To illustrate this further, an examination for phase-change natural convection with smaller viscosity and larger thermal expansion coefficient was carried out, and the result is shown in Fig. 7. Here the viscosity and thermal expansion coefficient of *air* were adopted, which are $1.85*10^{-5}$ Pa·s and $3.43*10^{-3}$ K^{-1} respectively, but with other factors in the model remaining unchanged. It can be seen from Fig. 7 that the velocities driven by buoyancy force become much larger than those shown in Fig. 6, having an order of magnitude of 10^{-1} m/s. Then they are strong enough to produce dominant influence on heat transfer.

5.4 Effect of metal foam microstructures

Figure 8 shows a comparison of temperature differences (between $y = 8$ mm and $y = 0$ mm) among three different metal-foam samples, each with either 95% or 85% porosity and with pore sizes of either 10 or 30 pores per inch (ppi). It shows that after an initial rise in temperature difference, there is a relatively constant temperature difference. This is followed by a rapid drop at around $t = 1200$s, due to melting beginning so that the phase change phenomenon enhances heat transfer performance. As time increases and melting continues, temperature differences stay relatively constant for a considerable time. Once the PCM near heating wall has finished absorbing the latent heat of fusion, the temperature differences rise rapidly. However, at this moment, the PCM at $y = 8$ mm has not finished the phase change process and still keeps a constant temperature of 58ºC. As time increases further, this part of PCM finishes the phase change process and consequently its temperatures rise dramatically around $t = 3000$s, resulting in a decrease of temperature differences.

When heat flux density is fixed, smaller temperature difference means higher heat transfer rate. The temperature differences in Fig. 8 can be transformed into equivalent thermal conductivities as shown in Fig. 9 by using Eq. (31), which is based on Fourier's Law:

$$U_{eq} = q\frac{\Delta d}{\Delta T} \tag{31}$$

It can be seen from Fig. 9 that the metal-foam sample with smaller pore size (30 ppi) has better heat transfer performance than the sample of 10 ppi. This is reasonable because smaller pore size results in larger contact area between the PCM and metal ligaments for transferring heat.

Figure 9 also shows that the metal-foam sample with 85% porosity can achieve better heat transfer performance than that with 95% porosity. This is reasonable because the former has more solid structures, which results in higher effective thermal conductivity; thus it can transfer heat flux more efficiently from the bottom surface to PCMs through the metal foam skeleton.

In summary, metal-foam samples with smaller pore size and porosity can achieve

better heat transfer performance than those with larger pore size and porosity.

5.5 PCM Temperature profiles during phase change process

Figures 10(a) – (d) show the evolution of temperature profiles for the metal-foam sample with 95% porosity and 10 ppi during melting process. Fig. 10(a) shows its temperature profiles at $t = 976.5$ s. At this time, the maximum temperature of the PCM in the whole region is 57ºC which is still just below melting point (58ºC). When $t = 1108.3$ s, a small part of PCM near bottom side has been heated up to melting point (58ºC) and begins to melt gradually, as shown by those isotherms in Fig. 10(b). It also shows that the left and right parts of PCMs near bottom side have not yet begun to melt, because the PCM here is losing heat to atmosphere through the left and right boundary and consequently has not acquired enough heat to before melting.

As time increases, the melting front gradually moves upwards, meaning more and more of the PCM is being melted, as shown in Fig. 10(c). The PCM temperature profiles when $t = 5859.0$s are shown in Fig. 10(d). At this time, all of the PCM has been fully heated into liquid state, with the minimum and maximum temperatures being 72ºC and 92ºC.

6. Conclusions

The numerical results have shown good agreement with experimental data, even though the PCM (RT58) used in the experiments does not have a fixed melting point, as assumed in the model. When comparing samples having metal foams embedded into PCM with a pure PCM sample, it was found that the addition of metal foams can considerably enhance PCM heat transfer performance (about 10 times) through effectively transferring heat from the metal skeleton to the PCM.

It was found from the simulations that the velocity driven by the buoyancy force is not strong enough to produce dominant influence on heat transfer in the PCM. This is due to the high viscosity (about 1000 times higher than air) and low thermal expansion coefficient (30 times lower than air) of RT58, as well as the high flow resistance in metal foams. The simulation results also indicated that metal foams with smaller pore size and porosity can achieve better heat transfer performance than those with larger pore size and porosity. In addition, a series of detailed evolutions of velocity and temperature

distributions have been obtained; these illustrate clearly the phase change processes of the PCM.

Acknowledgements

References

[1] Zalba B, Marin JM, Cabeza LF, Mehling H. Review on thermal energy storage with phase change: materials, heat transfer analysis and applications. Applied Thermal Engineering 2003;23:251-283.

[2] Sharma A, Tyagi VV, Chen CR, Buddhi D. Review on thermal energy storage with phase change materials and applications. Renewable and Sustainable Energy Review 2009;13:318-345.

[3] Solomon AD. Design criteria in PCM wall thermal storage. Energy 1979;4:701-709.

[4] Salyer IO, Sircar AK. Phase change materials for heating and cooling of residential buildings and other applications, In: Proceedings of the 25th Intersociety Energy Conversion Engineering Conference – IECEC'90, 1990:236–243.

[5] Neeper DA. Thermal dynamics of wallboard with latent heat storage. Solar Energy 2000; 68:393–403.

[6] Medina MA, King JB, Zhang M. On the heat transfer rate reduction of structural insulated panels (SIPs) outfitted with phase change materials (PCMs). Energy 2008;33:667-678.

[7] Buddhi D. Thermal performance of a shell and tube PCM storage heat exchanger for industrial waste heat recovery, presented at solar world congress, Taejon, Korea, August 24th – 30th, 1977.

[8] Mettawee EBS, Assassa GMR. Experimental study of a compact PCM solar collector. Energy 2006;31:2958-2968.

[9] Michels H, Pitz-Paal R. Cascaded latent heat storage for parabolic trough solar power plants. Solar Energy 2007;81:829-837.

[10] Shatikian V, Ziskind G, Letan R. Numerical investigation of a PCM-based heat sink with internal fins: Constant heat flux. International Journal of Heat and Mass Transfer 2008;51:1488-1493.

[11] Domanski R, El-Sebaii AA, Jaworski M. Cooking during off-sunshine hours using PCMs as storage media. Energy 1995;20:607-616

[12] Sharma SD, Iwata T, Kitano H, Sagara K. Thermal performance of a solar cooker based on an evacuated tube solar collector with a PCM storage unit. Solar Energy 2005;78:416-426.

[13] El-Sebaii AA, Al-Ghamdi AA, Al-Hazmi FS, Faidah AS. Thermal performance of a single basin solar still with PCM as a storage medium, Applied Energy 2009;86:1187-1195.

[14] Tyagi VV, Buddhi D. Thermal cycle testing of calcium chloride hexahydrate as a possible PCM for latent heat storage. Solar Energy Materials and Solar Cells 2008;92:891-899.

[15] El-Sebaii AA, Al-Heniti S, Al-Agel F, Al-Ghamdi AA, Al-Marzouki F. One thousand thermal cycles of magnesium chloride hexahydrate as a promising PCM for indoor solar cooking. Energy Conversion and Management 2011;52:1771-1777.

[16] Mettawee ES, Assassa GMR. Thermal Conductivity enhancement in a Latent Heat Storage System. Solar Energy 2007;81:839-845.

[17] Mills A, Farid M, Selman JR, Al-Hallaj S. Thermal conductivity enhancement of phase change materials using a graphite matrix. Applied Thermal Engineering 2006;26:1652-1661.

[18] Zhao CY, Lu W, Tian Y. Heat transfer enhancement for thermal energy storage using metal foams embedded within phase change materials (PCMs). Solar Energy 2010;84:1402-1412.

[19] Hamada Y, Otsu W, Fukai J, Morozumi Y, Miyatake O. Anisotropic heat transfer in composites based on high-thermal conductive carbon fibers. Energy 2005;30:221-233.

[20] Calmidi VV. Transport Phenomena in High Porosity Metal Foams, Ph.D thesis, University of Colorado 1998.

[21] Zhao CY, Kim T, Lu T J, Hodson H P. Thermal transport in high porosity cellular metal foams. Journal of Thermophysics and Heat Transfer 2004;18:309-317.

[22] Calmidi VV, Mahajan RL. Forced convection in high porosity metal foams. ASME Transactions – Journal of Heat Transfer 2000;122:557-565.

[23] Boomsma K, Poulikakos D. On the effective thermal conductivity of a three-dimensionally structured fluid-saturated metal foam. International Journal of Heat and Mass Transfer 2001;44:827 – 836.

[24] Zhao CY, Lu TJ, Hodson HP. Natural convection in metal foams with open cells. International Journal of Heat and Mass Transfer 2005;48:2452-2463.

[25] Siahpush A, O'Brien J, Crepeau J. Phase Change Heat Transfer Enhancement Using Copper Porous Foam. ASME Transactions - Journal of Heat Transfer 2008;130:082301-1 to 082301-11.

[26] Krishnan S, Murthy JY, Garimella SV. A Two-temperature Model for Solid-liquid Phase Change in Metal Foams. ASME Transactions – Journal of Heat Transfer 2005;127:997-1004.

[27] Tian Y, Zhao CY. Thermal Analysis in Phase Change Materials (PCMs) Embedded with Metal Foams, In: Proceedings of the 14th International Heat Transfer Conference - IHTC14, paper number: IHTC14-22452, Washington DC, USA, August 8th – 13th, 2010.

[28] Zukauskas AA. Convective heat transfer in cross-flow, handbook of single-phase heat transfer. New York: Wiley; 1987.

[29] Patankar S. Numerical heat transfer and fluid flow. New York: Hemisphere Publishing Corporation; 1980.

[30] Stritih U. An experimental study of enhanced heat transfer in rectangular PCM thermal storage. International Journal of Heat and Mass Transfer 2004;47:2841–2847.
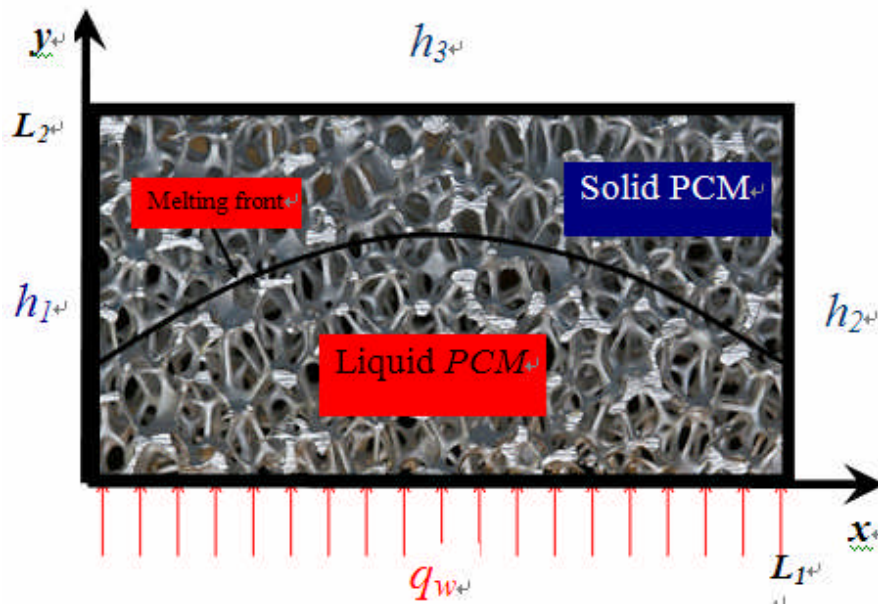
Figure Captions

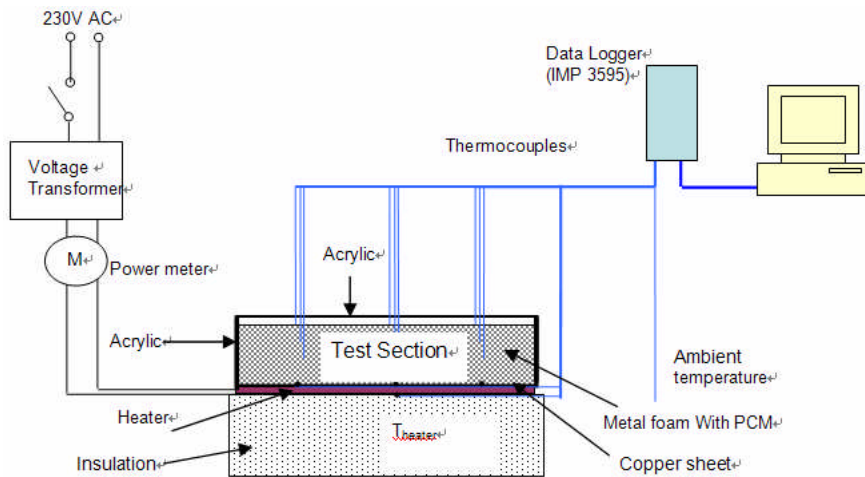Figure 1: Illustration of PCMs embedded into metal foams.

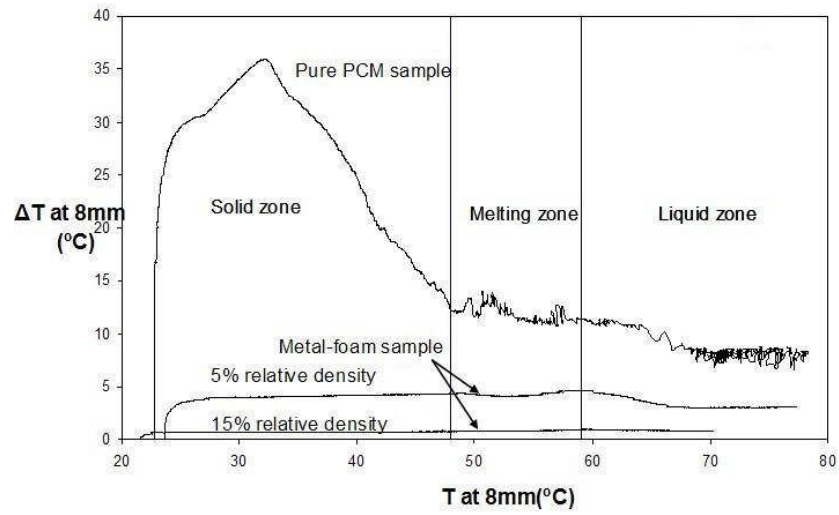Figure 2: Schematic of the experimental test rig.

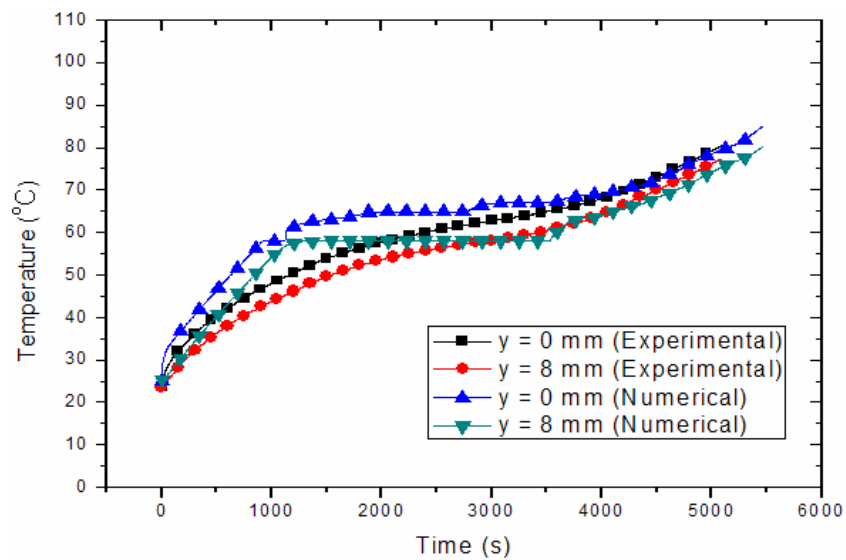Figure 3: A comparison between the pure PCM sample and metal-foam samples.

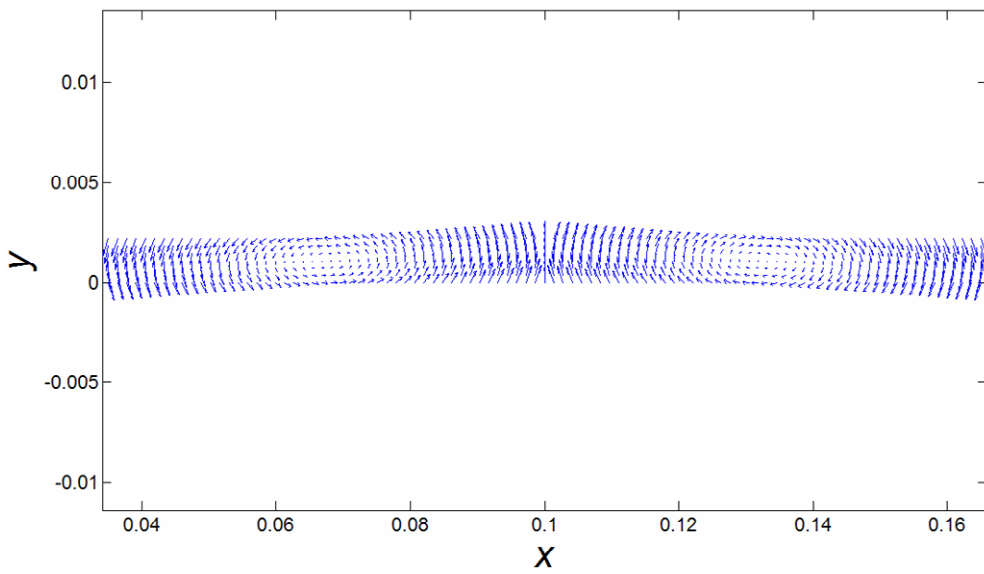Figure 4: A comparison between numerical results and experimental data.

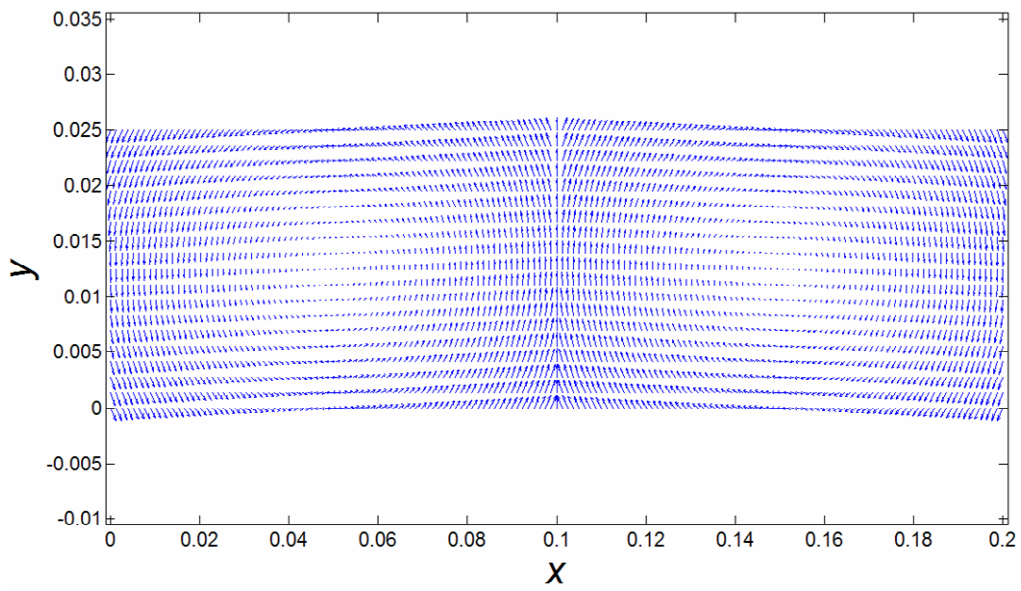Figure 5: Velocity profile of natural convection ($t = 1108.3$ s).

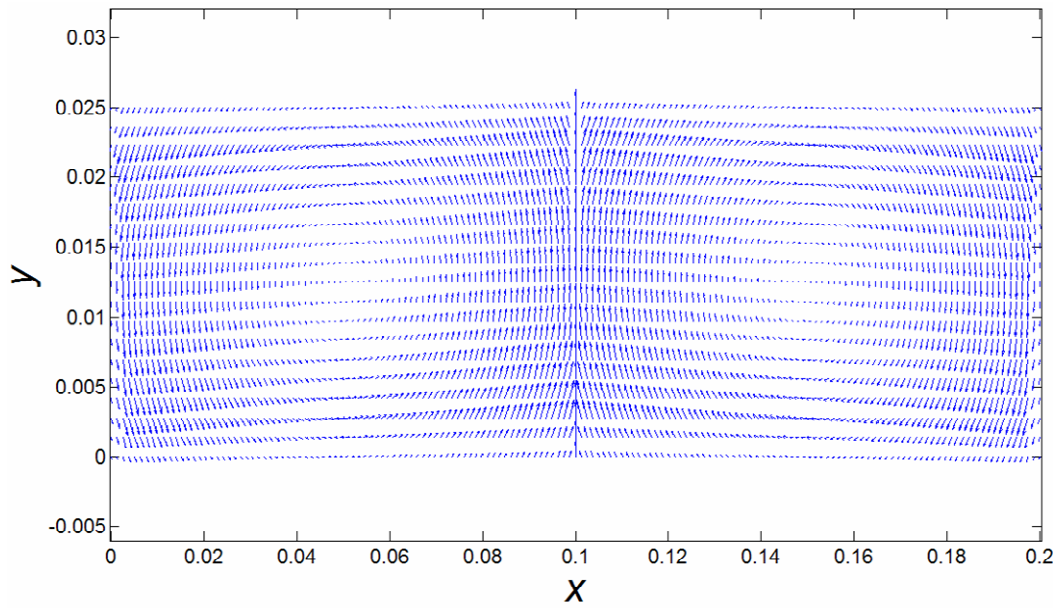Figure 6: Velocity profile of natural convection ($t = 5859.0$ s).

Figure 7: Velocity profile for lower viscosity and higher thermal expansion rate.

Figure 8: A comparison of temperature differences among different porosities and pore sizes.
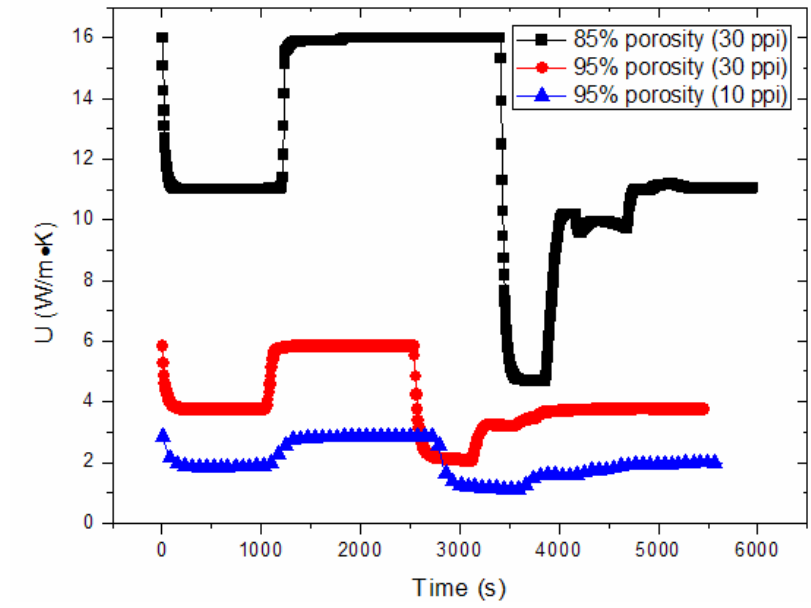
Figure 9: A comparison of equivalent thermal conductivities among different porosities and pore sizes.

Figure 10: Temperature profiles.

Fig. 1. Illustration of PCMs embedded into metal foams.

Fig. 2. Schematic of the experimental test rig.

Fig. 3. A comparison between the pure PCM sample and metal-foam samples.

Fig. 4. A comparison between numerical results and experimental data.

Fig. 5. Velocity profile of natural convection ($t = 1108.3$ s).

Fig. 6. Velocity profile of natural convection ($t = 5859.0$ s).

Fig. 7. Velocity profile for lower viscosity and higher thermal expansion rate.
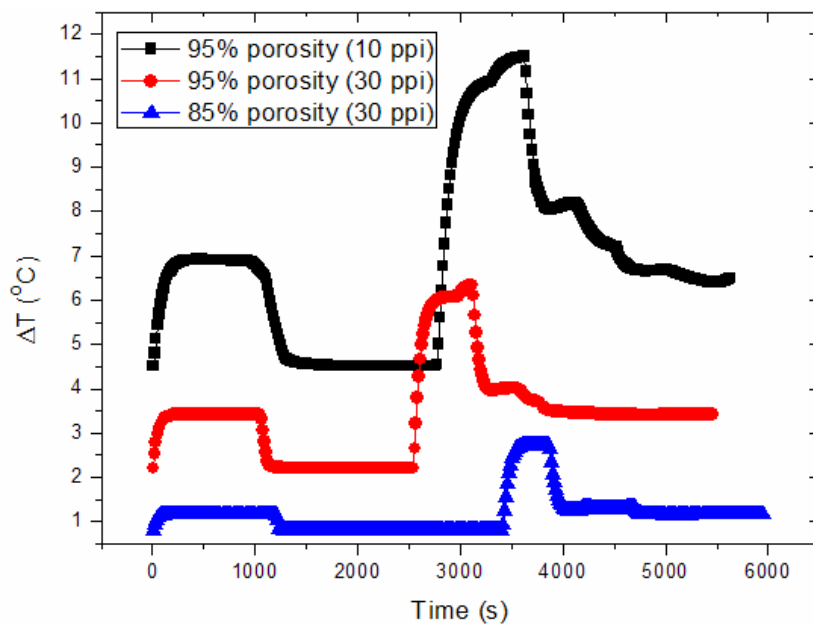
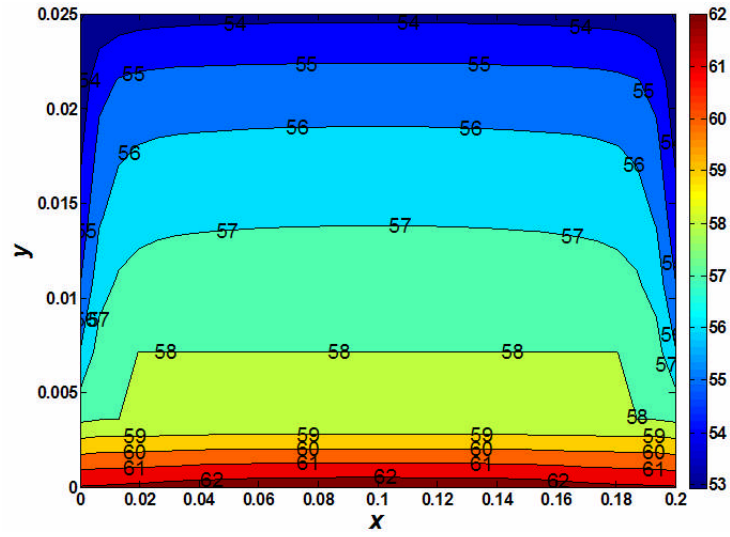**Fig. 8.** A comparison of temperature differences among different porosities and pore sizes.

Fig. 9. A comparison of equivalent thermal conductivities among different porosities and pore sizes.
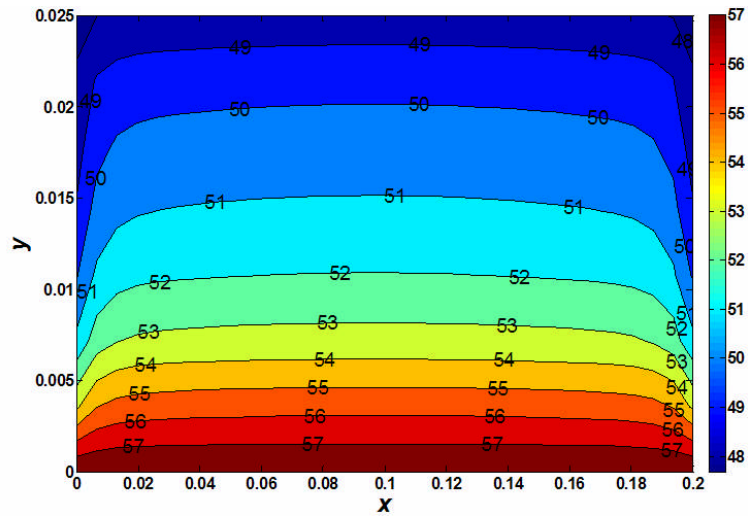
(a) $t = 976.5\ s$.
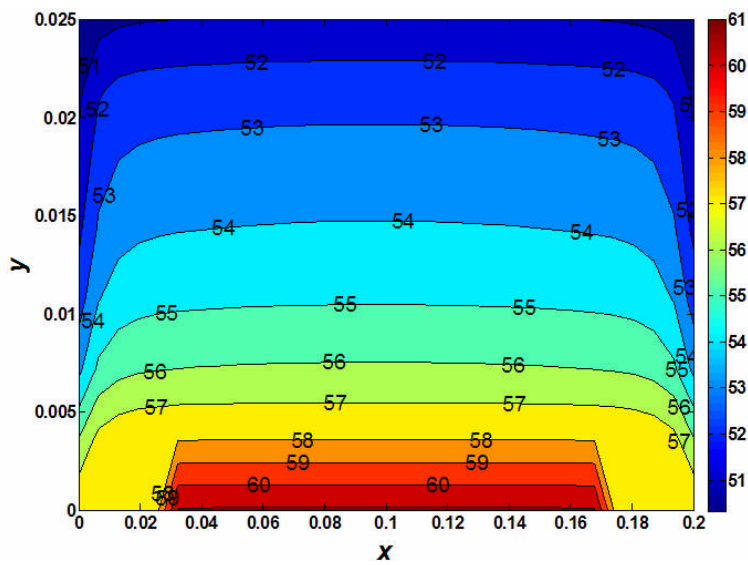
(b) $t = 1108.3\ s$.

(c) *t* = 1318.3 *s.*
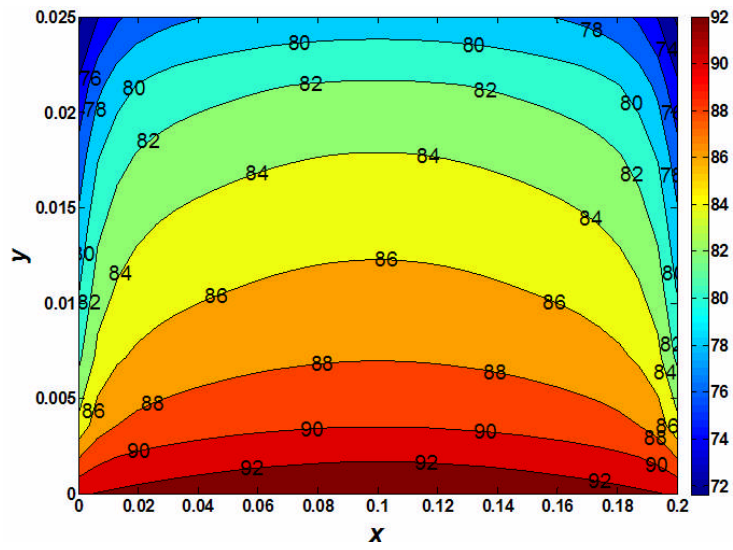
(d) *t* = 5859.0 *s.*

Fig. 10. Temperature profiles.